Chemical Engineering Journal 155 (2009) 905–909

Contents lists available at ScienceDirect

Chemical Engineering Journal

journal homepage: www.elsevier.com/locate/cej

# High-efficient microwave synthesis and characterisation of $SrSnO_3$

Jörg Bohnemann[a,b], Rafael Libanori[b], Mário L. Moreira[b,*], Elson Longo[c]

[a] Department of Chemistry, Westfälische Wilhelms-University Münster, 48149 Münster, Germany
[b] Laboratório Interdisciplinar de Eletroquímica e Cerâmica (LIEC), Universidade Federal de São Carlos (UFSCar), P.O. Box 676, Rodovia Washington Luis, Km 235, 13565-905, São Carlos, SP, Brazil
[c] Laboratório Interdisciplinar de Eletroquímica e Cerâmica (LIEC), Instituto de Química, Universidade Estadual Paulista (UNESP), Rua Francisco Degni, s/n, 14800-900, Araraquara, SP, Brazil

ARTICLE INFO

*Article history:*
Received 29 May 2009
Received in revised form 27 August 2009
Accepted 1 September 2009

*Keywords:*
$SrSnO_3$
Microwave
Nanostructures
Photoluminescence

ABSTRACT

Strontium stannate ($SrSnO_3$) nanostructures were obtained by microwave-assisted calcination of a $SrSn(OH)_6$ precursor powder. Compared to other conventional calcination methods mentioned in the literature, this procedure led to a remarkable decrease of the reaction time and the synthesis temperature owing to direct interaction of radiation with the material. X-ray diffraction (XRD), field-emission scanning electron microscopy (FE-SEM) and photoluminescence measurements were performed. A comparison of the characterisation results obtained by microwave and conventional methods was conducted, and differences concerning the properties of conventionally high-temperature calcined $SrSnO_3$ from that obtained by microwave-assisted calcination were observed. Furthermore, two different morphologies (*nanosticks* and *nanobrushes*) were obtained by a variation of the concentration of the reactants.

© 2009 Elsevier B.V. All rights reserved.

## 1. Introduction

Perovskite stannates $MSnO_3$ (with M = Ca, Sr or Ba) are technically and industrially interesting ceramics. Besides their useful dielectric properties, their applications as thermally capable capacitors and semiconductor sensors for humidity and gases have already been reported [1–5]. Due to its relevance, efficient synthesis routes of stannates are of particular interest.

The stannates have already been synthesised successfully using several methods, such as high-temperature solid state reactions of mixtures of $M(NO_3)_2/SnO_2$ or $MCO_3/SnO_2$ powders at 1000–1200 °C for $SrSnO_3$ [6–8] and at 1000–1450 °C for other stannates [9–11]. Apart from these ceramic routes, those stannates can also be prepared via sol–gel techniques [12] or the thermal decomposition of oxalates [13]. However, these two alternative techniques also require temperatures of 800 °C or 1000 °C, respectively. Despite the many syntheses and characterisations of strontium stannate ($SrSnO_3$) which have frequently been under investigation in the literature [6–8], low temperature and short time synthesis methods are rare [14,15]. All above mentioned ceramic routes for the preparation of the stannates have in common long synthesis times (up to 16 h). Therefore, an alternative cost-efficient synthesis route using shorter times and lower temperatures is clearly demanded.

In general, microwave-assisted synthesis is an interesting approach which is used to synthesise many inorganic compounds such as metals, oxides, chalcogenides and phosphates [16], demonstrating the scope of application of this technology. Microwave-assisted hydrothermal syntheses (HTMW method) have also been performed for several compositions [17].

We hereby report a novel and highly efficient approach for the synthesis of strontium stannate at significantly lower temperatures and shorter reaction times. This improved synthesis was realised by introducing a microwave-assisted calcination method instead of conventional high-temperature calcination. In this paper, we present the results of XRD, FE-SEM and photoluminescence measurements of strontium stannates, obtained by microwave-assisted calcinations along with a comparison with results obtained by conventional calcinations.

## 2. Experimental details

The synthesis of $SrSnO_3$ consists in obtaining the precursor $SrSn(OH)_6$ by an aqueous chemical route, which was sequentially submitted to a microwave-assisted calcination. The precursor was synthesised using the following reagents: tin chloride ($SnCl_4{\cdot}5H_2O$, 98%, Aldrich) and strontium chloride ($SrCl_2{\cdot}6H_2O$, 99%, Aldrich). Water was boiled before its use to reduce the amount of $CO_2$. Additionally, an inert gas atmosphere was used throughout the synthesis, reducing the formation of by-products, such as $SrCO_3$. The syntheses were performed at room temperature. $SrSn(OH)_6$ *nanosticks* were synthesised by preparing a mixture of $SnCl_4{\cdot}5H_2O$

* Corresponding author. Tel.: +55 16 3351 8214.
*E-mail address:* mlucio@liec.ufscar.br (M.L. Moreira).

1385-8947/$ – see front matter © 2009 Elsevier B.V. All rights reserved.
doi:10.1016/j.cej.2009.09.004

(12 mmol) and $SrCl_2{\cdot}6H_2O$ (12.6 mmol) in 20 mL $H_2O$, corresponding to a 0.60 M ($Sn^{4+}$)/0.63 M ($Sr^{2+}$) solution. This mixture was added slowly to 20 mL of an 8 M solution of sodium hydroxide. During this step, continuous magnetic stirring was maintained, and a white powder was formed immediately. After filtering, washing and drying at 70 °C, the desired precursor $SrSn(OH)_6$ was obtained. Another morphology of the precursor, $SrSn(OH)_6$ *nanobrushes* were synthesised reducing the concentration of the reactants. A mixture of $Sn^{4+}$ (3.8 mmol) and $Sr^{2+}$ (4.0 mmol) in 25 mL $H_2O$ corresponding to 0.15 M ($Sn^{4+}$)/0.16 M ($Sr^{2+}$) solution was added slowly to 25 mL of an 8 M solution of NaOH. The slight excess of $Sr^{2+}$ was used to compensate the formation of $SrCO_3$ which is difficult to avoid completely. The water content of the highly hygroscopic tin chloride was determined by thermogravimetric measurements.

The precursors were exposed to simple microwave processing in a ceramic crucible at different times and temperatures. In all cases, a heating rate of 20 °C/min was used. To obtain highly crystalline strontium stannate ($SrSnO_3$), a calcination time of at least 10 min at 500 °C was necessary.

All XRD patterns were collected using a Rigaku D/Max 2500PC X-ray diffractometer with a rotary anode using Cu Kα (λ = 1.5406 Å) radiation operating at 150 kV and 40 mA in the 2θ range from 5° to 75° with a step scan mode of 0.02° using Jade 5 software. Nanostructures were characterised by field-emission scanning electron microscopy (FE-SEM) performed on a Zeiss Supra™ 35 device using Smart SEM 5 software. Photoluminescence emission was detected using a Tharmal Jarrel-Ash Monospec 27 monochromator and a Hamamatshu R446 photomultiplier. The Coherent Innova multi-line Krypton ion laser had an output power of 250 mW and a 350.7 nm (3.54 eV) exciting wavelength. The microwave device featured a frequency of 2.45 GHz. UV–visible measurements for band gap determinations were performed on a Varian Cary 500 UV–visible NIR spectrophotometer using reflectance mode. All measurements were carried out at room temperature.

## 3. Results and discussion

Fig. 1 illustrates the XRD pattern identified by JCPDS No. 09-0086, confirming the formation of the precursor $SrSn(OH)_6$. The system is highly susceptible to the formation of by-product phases [18]. For instance, we observed that an excess of $SnO_2$ can lead to the formation of $Sr_2SnO_4$ during the calcination step (data not shown). Moreover, the amount of the $SrCO_3$ phase can be decreased

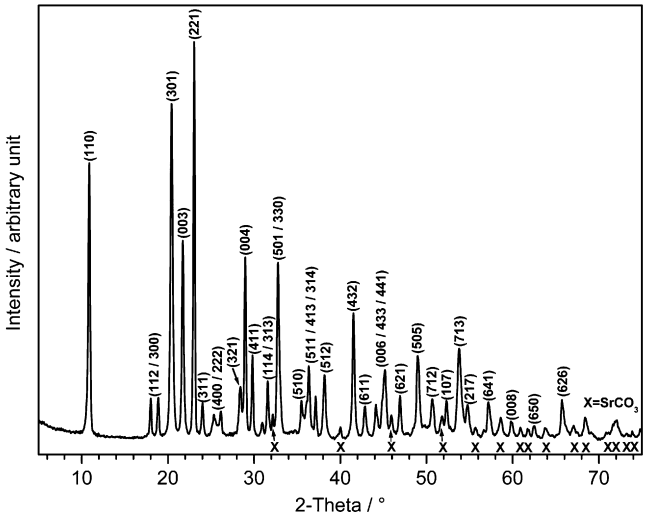


**Fig. 1.** XRD pattern of the $SrSn(OH)_6$ precursor. The marked peaks (X) indicate impurities caused mainly by a $SrCO_3$ phase.

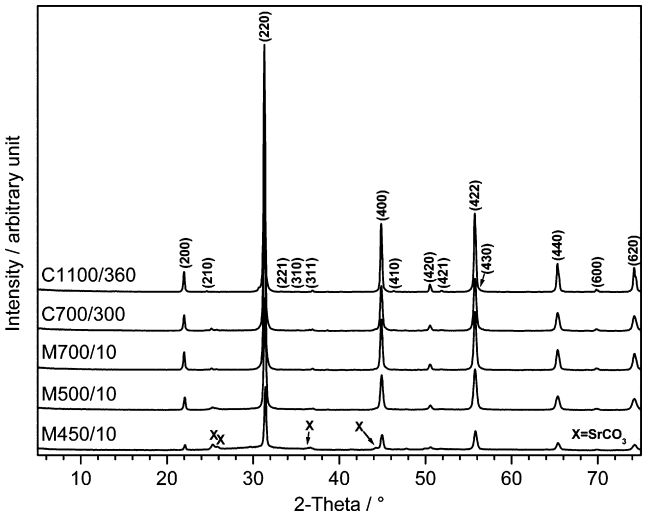


**Fig. 2.** XRD pattern of $SrSnO_3$ samples M450/10, M500/10, M700/10, C700/300 and C1100/360. The marked peaks (X) indicate the formation of a $SrCO_3$ phase.

using cooked and $N_2$-purged water. The marked peaks in Fig. 1 show the presence of the additional phase $SrCO_3$. $SrSn(OH)_6$ features a hexagonal structure in the *Pn3m* space group [19].

Fig. 2 compares the XRD patterns of $SrSnO_3$ samples obtained by calcinations in the conventional and the microwave oven at different times and temperatures. The formation of the $SrSnO_3$ phase was identified by JCPDS No. 22-1442. The treatment of the precursor leads to the formation of a $SrSnO_3$ phase by dehydration, as shown in Eq. (1)

$$SrSn(OH)_6 \xrightarrow[-3H_2O]{\Delta} SrSnO_3 \quad (1)$$

The calcination of $SrSn(OH)_6$ performed at 500 °C in the microwave oven provided the desired phase $SrSnO_3$ (sample M500/10) after only 10 min. However, calcination temperatures below 500 °C for 10 min in the microwave (e.g., 450 °C (sample M450/10)), did not promote the complete crystallisation of the $SrSnO_3$ phase. This sample M450/10 also featured $SrCO_3$ as a secondary phase. Considering the XRD results, the application of higher temperatures than for sample M500/10 is not necessary, as calcinations at 700 °C for 10 min in the microwave (sample M700/10) and 300 min in the conventional oven (sample C700/300) did not show noteworthy differences. Besides, sample M500/10 was completed successfully whereas other samples obtained by conventional processing at 500 °C (e.g., after 210 min, data not shown) did not feature a complete crystallisation process. We can therefore confirm that, in this case, calcinations in the microwave can be completed at comparatively shorter times than in the conventional oven when the same temperature is considered. Excluding sample M450/10, all samples report an orthorhombic structure in the *Pbnm* space group (see Fig. 3) composed of octahedral Sn and dodecahedral Sr sites. A typical conventional calcination of $SrSnO_3$ reported in the literature was performed at 1100 °C for 360 min [6]. This procedure was chosen as a reference sample (C1100/360) in order to compare the results of conventional and microwave-assisted syntheses.

The efficiency demonstrated by using microwave-assisted calcinations is related to a more effective heat transfer process. Thus, microwave radiation interacts directly with the crystallisation water of the $SrSn(OH)_6$ precursor by irradiation, favouring the permeation of the sample significantly faster and with a higher efficiency than the thermal energy provided by the convection and conduction process used by conventional ovens. In addition, as microwave radiation is distributed more evenly within the sample,

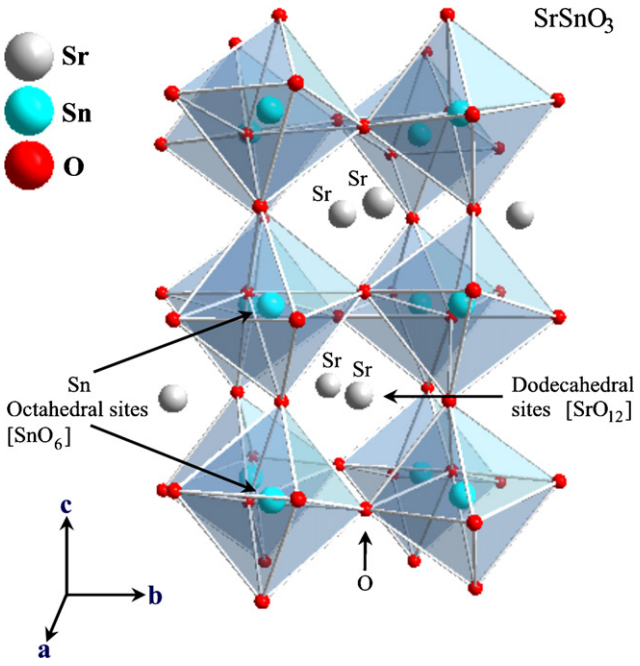


**Fig. 3.** Schematic model of $SrSnO_3$ *Pbnm* orthorhombic structure, reporting octahedral $SnO_6$ and dodecahedral $SrO_{12}$ clusters.

high thermal gradients are avoided during the calcination. Consequently, the introduction of microwave-assisted processing often leads to a decrease in the reaction time and calcination temperature [20,21].

As already mentioned, we have obtained two different morphologies of nanoparticles by varying the ion concentration of the reactants. The development of the particular morphology is determined during the formation of the precursor. Fig. 4 shows FE-SEM images of $SrSnO_3$ nanoparticles composed of *nanosticks* whereas Fig. 5 illustrates FE-SEM images of $SrSnO_3$ nanostructures self-assembled on *nanobrushes*, obtained by microwave-assisted (left) and conventional (right) calcinations processes, respectively. Those self-assembled structures usually form a specific architecture by aggregation; in the case of Fig. 5, a mesocrystalline brush-like morphology is formed.

The *nanosticks* feature diameters of 200 nm up to 1.5 μm and lengths of several μm each unit (Fig. 4, images a–f), irrespective of the calcination method. Concerning the surface of samples M500/10 and C1100/360, mentionable differences can be observed (see images c and f). The surface of $SrSnO_3$ *nanosticks* obtained from the microwave (a–c) is smoother than the material from the conventional oven (d–f), where we observed the formation of small crystals (f) which originate the single *nanostick* elements. Thus, such peculiarities on the surface of the nanosticks are obviously related to the calcination temperature, as we observed the formation of cracks on the surface of *nanosticks* of sample M700/10 (data

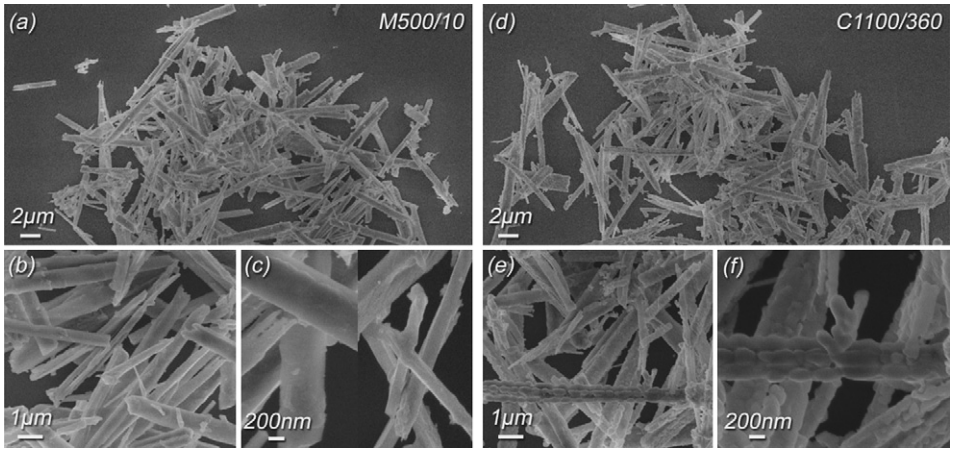


**Fig. 4.** FE-SEM images of $SrSnO_3$ *nanosticks* by microwave-assisted (left: sample M500/10) and conventional calcinations (right: sample C1100/360) at different magnifications.

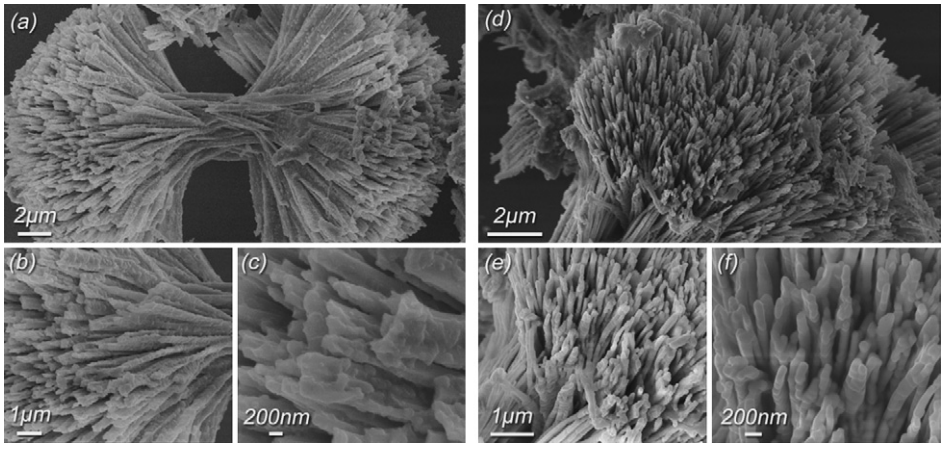


**Fig. 5.** FE-SEM images of $SrSnO_3$ *nanobrushes* by microwave-assisted (left) and conventional calcinations (right) at different magnifications. The samples were obtained under the same conditions like in Fig. 4 (10 min at 500 °C and 360 min at 1100 °C, respectively).

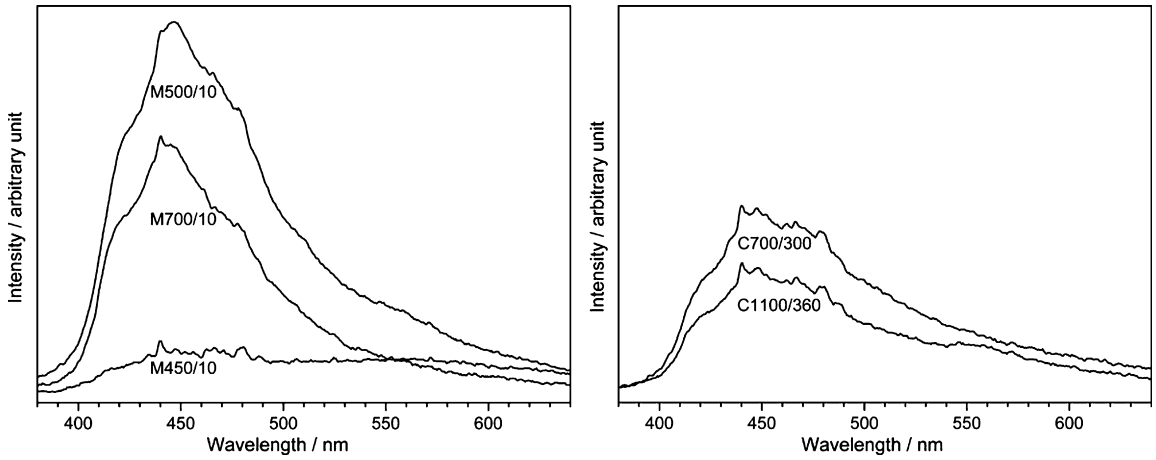


**Fig. 6.** Photoluminescence emission spectra of $SrSnO_3$ *nanosticks* by microwave-assisted (left: samples M450/10, M700/10 and M500/10) and by conventional calcinations (right: samples C1100/360 and C700/300).

not shown). However, the *nanostick* precursor does not feature these characteristics, as well as sample M500/10.

*Nanobrushes* (Fig. 5, images a–f) are obtained only by syntheses at comparatively lower ion concentrations, in this case 0.15 M ($Sn^{4+}$)/0.16 M ($Sr^{2+}$). The *nanobrushes* obtained by microwave-assisted processing at 500 °C for 10 min (a–c) show a scale-like surface whereas the structures from conventional calcinations (d–f) are made of many rod-like nanoelements, mainly showing a width of approximately 200 nm. This mesostructure is obtained by conventional processing at 1100 °C for 360 min and appears to be formed of small crystals (f), comparable to sample C1100/360, which has been calcined under identical conditions. Thus, the nanoelements are self-assembled to originate the *nanobrush*.

Perovskite-based materials ($ABO_3$) consist of a corner-linked $BO_6$ octahedra network enclosed by large dodecahedral cavities ($AO_{12}$). Strontium stannate is composed of $SnO_6$ octahedral and $SrO_{12}$ dodecahedral clusters [22,23], as illustrated in Fig. 3. For those materials, the photoluminescence (PL) properties are related to the appearance of intermediated states (recombination centres) as a consequence of a redistribution in the density of states concerning both $SnO_6$ and $SrO_{12}$ clusters in the strontium stannate network. The appearance of intermediated states are a result of distortions provoked in both clusters due to the direct network dependence between them; i.e., if any distortion occurs in one cluster, another cluster will be distorted as well, leading to new configurations of the density of states for each sample.

In order to describe the PL properties of crystalline structures, it is convenient to consider three different structural degrees of order–disorder: short, medium and long-range order. For $ABO_3$ perovskites, the medium-range order is related to the distortion in the clusters located in the network. The short-range order concerns the local arrangements of each cluster and the long-range order is represented by the three-dimensional periodic repetition of the clusters within the network. The PL emission spectra of $SrSnO_3$ samples obtained in the microwave and conventional oven are shown in Fig. 6. It can be seen that samples M450/10 and C1100/360 present the lowest PL emissions. These results may arise from the different structural order featured by these two samples. The former underwent an incomplete crystallisation process whereas the latter is highly crystalline (see Fig. 2). It is well-known that PL emission is a consequence of the ratio among an order–disorder degree [24–28]. From this point of view, high-ordered as well as low-ordered structures avoid the formation of recombination centres, which are indispensable for the presence of PL emission.

Considering the microwave-assisted calcined samples M500/10 and M700/10 (Fig. 6, left), it is noted that a long-range order is present, but also a certain disorder degree remains in their structure as evidenced by their PL emissions. In this context, the structural order of sample M700/10 is higher than in the case of sample M500/10, therefore the PL emission is lower. This effect can also be observed by considering conventionally calcined samples (Fig. 6, right), where sample C1100/360 shows a lower PL emission than sample C700/300. Here again a higher calcination temperature leads to a comparable lower PL emission. It is noted that a long-range and short-range order is present in the case of samples M500/10, M700/10, C700/300 and C1100/360 as indicated by XRD patterns (Fig. 2) and Raman spectra (see Supporting Information). However, according to the PL emission in some cases, also a medium-range disorder can still be present in the crystalline structures. The calcination time, temperature and the oven type are regarded as important parameters concerning the PL behaviour. Besides, the broad spectra observed in all samples are originated from a multiphotonic process, in which several states are formed inside of the band gap, allowing numerous different energetic transitions among them. Hence, the PL emission leads to a broad band covering a large part of visible spectra.

As mentioned above, the PL emission can be ascribed to the presence of medium-range order–disorder in the crystalline structures discussed and, therefore, the formation of states within the band gaps. This approach is suitable because the excitation energy (3.54 eV) normally is smaller than the original band gap, avoiding a direct transition from the valence to the conduction band. The band gap value of $SrSnO_3$ reported in the literature is 4.1 eV [29] which is 0.34 eV higher than the result obtained in our work for sample C1100/360 (3.76 eV) and 0.47 eV higher for sample M500/10 (3.63 eV). Therefore, we can conclude that the conventional oven method has a larger capacity to eliminate the shallow or more energetic defects while the microwave oven is unable to eliminate them [25]. Furthermore, the microwave method is highly efficient in the rapid crystallisation of the $SrSnO_3$ network. These behaviours are denoted by the displacement of the PL centre from 444 nm (high energetic) for the microwave samples (Fig. 6, left) towards 460 nm (less energetic) for samples heat treated in the conventional oven (Fig. 6, right). Different PL emission bands are observed considering the samples, and the necessary conditions for the appearance of states within the band gap are present [22,30]; e.g., sample M500/10 shows a more disordered structure than sample C1100/360, denoted by the lower band gap values. Besides, the asymmetry of the PL emission bands is possibly related to electron–phonon coupling [31]. This leads to a decrease of the thermal occupancy in high-ordered vibrational states of the material.

## 4. Conclusion

In conclusion, the microwave-assisted calcination method turned out to be a high-efficient approach to obtain $SrSnO_3$ samples at significant lower temperatures and shorter reaction times when compared to conventional calcination procedures. It was also observed that the calcination method plays an important role on the photoluminescent properties as well as on the surface morphology and the crystallisation time of the $SrSnO_3$. The directed formation of different morphologies dependent from the reaction conditions could be demonstrated; this was achieved by a variation of ion concentration. The high PL emission of samples obtained by microwave-assisted calcination could be explained by the presence of medium-range disorder in their structures, whereas the samples treated in the conventional oven showed low PL emission, due to the presence of highly ordered structures. Consequently, the PL emission is a good approach to indicate the presence of medium-range disorder in the crystalline structures, and, therefore, the formation of intermediate states within the band gaps.

## Acknowledgements

Support of the project from IAESTE/DAAD and financial support by the Brazilian research financing institutions CAPES, CNPq and FAPESP/CEPID 98/14324-0 is gratefully acknowledged. One of the authors (Bohnemann) thanks everybody at the LIEC São Carlos who contributed to this work by performing measurements or taking part in discussions. The authors are grateful to Prof. M.S. Li (USP), providing the equipment for the photoluminescence measurements.

## Appendix A. Supplementary data

Supplementary data associated with this article can be found, in the online version, at doi:10.1016/j.cej.2009.09.004.

## References

[1] Y. Shimizu, M. Shimabukuro, H. Arai, T.J. Seiyama, Humidity-sensitive characteristics of $La^{3+}$-doped and undoped $SrSnO_3$, Electrochem. Soc. 136 (1989) 1206–1210.
[2] T. Ishihara, H. Fujita, Y. Takita, Effects of Pt addition for $SrSnO_3$–$WO_3$ capacitive type sensor on NO detection at high temperature, Sens. Actuators B 52 (1998) 100–106.
[3] U. Lampe, J. Gerblinger, H. Meixner, Nitrogen oxide sensors based on thin films of $BaSnO_3$, Sens. Actuators B 26 (1995) 97–98.
[4] A. Kumar, R.N.P. Choudhary, B.P. Singh, A.K. Thakur, Effect of strontium concentration on electrical conduction properties of Sr-modified $BaSnO_3$, Ceram. Int. 32 (2006) 73–83.
[5] M. Pelino, C. Cantalini, Principles and applications of ceramic humidity sensors, Active Passive Elec. Comp. 16 (1994) 69–87.
[6] D. Chen, J. Ye, $SrSnO_3$ nanostructures: synthesis, characterization, and photocatalytic properties, J. Chem. Mater. 19 (2007) 4585–4591.
[7] O.M. Parkash, K.D. Mandal, C.C. Christopher, M.S. Sastry, D.J. Kumar, Preparation and characterization of strontium stannate, $SrSnO_3$, Mater. Sci. Lett. 13 (1994) 1616–1617.
[8] A.M. Azad, L.L.W. Shyan, P.T. Yen, Characterization of $BaSnO_3$-based ceramics. Part 1. Synthesis, processing and microstructural development, J. Alloys Compd. 282 (1999) 109–124.
[9] A.M. Azad, N.C. Hon, Synthesis, processing and microstructural characterization of $CaSnO_3$ and $SrSnO_3$ ceramics, J. Alloys Compd. 270 (1998) 95–106.
[10] H. Mizoguchi, P.M. Woodward, C.-H. Park, D.A. Keszler, Strong near-infrared luminescence in $BaSnO_3$, J. Am. Chem. Soc. 126 (2004) 9796–9800.
[11] M.G. Smith, J.B. Goodenough, A. Manthiram, R.D. Taylor, W. Peng, C.W. Kimball, Tin and antimony valence states in $BaSn_{0.85}Sb_{0.15}O_{3-\delta}$, J. Sol. State Chem. 98 (1992) 181–186.
[12] N. Sharma, K.M. Shaju, G.V. Subba Rao, B.V.R. Chowdari, Anodic behaviour and XPS of ternary tin oxides, J. Power Sources 139 (2005) 250–260.
[13] M. Bao, W. Li, P.J. Zhu, Study on the dielectric properties of oxide-doped $Ba(Ti,Sn)O_3$ ceramics prepared from ultrafine powder, Mater. Sci. 28 (1993) 6617–6621.
[14] M. Leoni, M. Viviani, P. Nanni, V.J. Buscaglia, Low-temperature aqueous synthesis (LTAS) of ceramic powders with perovskite structure, Mater. Sci. Lett. 15 (1996) 1302–1304.
[15] C.P. Udawatte, M. Kakihana, M. Yoshimura, Low-temperature synthesis of pure $BaSnO_3$ and the $(Ba_{1-x})Sr_xSnO_3$ solid-solution by the polymerize complex method, Sol. State Ionics 128 (2000) 217–226.
[16] I. Bilecka, I. Djerdj, M. Niederberger, One-minute synthesis of crystalline binary and ternary metal oxide nanoparticles, Chem. Commun. 7 (2008) 886–888.
[17] S. Komarneni, R. Roy, Q.H. Li, Microwave-hydrothermal synthesis of ceramic powders, Mater. Res. Bull. 27 (1992) 1393–1405.
[18] M.L. Moreira, S.A. Pianaro, A.V.C. Andrade, A.J. Zara, Crystal phase analysis of $SnO_2$-based varistor ceramic using the Rietveld method, Mater. Charact. 57 (2006) 193–198.
[19] J.W. Kramer, S.A. Isaacs, V. Manivannan, Microwave-assisted metathesis synthesis of Schoenfliesite-type $MSn(OH)_6$ (M = Mg, Ca, Zn, and Sr) materials, J. Mater. Sci. 44 (2009) 3387–3392.
[20] V.S. Marques, L.S. Cavalcante, J.C. Sczancoski, D.P. Volanti, J.W.M. Espinosa, M.R. Joya, M. Santos, P.S. Pizani, J.A. Varela, E. Longo, Influence of microwave energy on structural and photoluminescent behavior of $CaTiO_3$ powders, Solid State Sci. 10 (2008) 1056–1061.
[21] D. Keyson, D.P. Volanti, L.S. Cavalcante, A.Z. Simões, I.A. Sousa, J.S. Vasconcelos, J.A. Varela, E. Longo, Domestic microwave oven adapted for fast heat treatment of $Ba_{0.5}Sr_{0.5}(Ti_{0.8}Sn_{0.2})O_3$ powders, E. Mater. Process. Technol. 189 (2007) 316–319.
[22] V.M. Longo, L.S. Cavalcante, R. Erlo, V.R. Mastelaro, A.T. de Figueiredo, J.R. Sambrano, S. de Lazaro, A.Z. Freitas, L. Gomes, N.D. Vieira, J.A. Varela, E. Longo, Strong violet-blue light photoluminescence emission at room temperature in $SrZrO_3$: joint experimental and theoretical study, Acta Mater. 56 (2008) 2191–2202.
[23] F. Farges, G.E. Brown, J.J. Rehr, Ti K-edge XANES studies of Ti coordination and disorder in oxide compounds: comparison between theory and experiment, Phys. Rev. B 56 (1997) 1809–1819.
[24] R.C. Lima, L.R. Macario, J.W.M. Espinosa, V.M. Longo, R. Erlo, N.L. Marana, J.R. Sambrano, M.L. dos Santos, A.P. Moura, P.S. Pizani, J. Andrés, E. Longo, J.A. Varela, Toward an understanding of intermediate- and short-range defects in ZnO single crystals. A combined experimental and theoretical study, J. Phys. Chem. A 112 (2008) 8970–8978.
[25] M.L. Moreira, J. Andrés, J.A. Varela, E. Longo, Synthesis of fine micro-sized $BaZrO_3$ powders based on a decaoctahedron shape by the microwave-assisted hydrothermal method, Cryst. Growth Design 9 (2009) 833–839.
[26] P.S. Pizani, E.R. Leite, F.M. Pontes, E.C. Paris, J.H. Rangel, E.J.H. Lee, E. Longo, P. Delega, J.A. Varela, Photoluminescence of disordered $ABO_3$ perovskites, Appl. Phys. Lett. 77 (2008) 824–826.
[27] E.R. Leite, L.P.S. Santos, N.L.V. Carreño, E. Longo, C.A. Paskocimas, J.A. Varela, F. Lanciotti Jr., C.E.M. Campos, P.S. Pizani, Photoluminescence of nanostructured $PbTiO_3$ processed by high-energy mechanical milling, Appl. Phys. Lett. 78 (2001) 2148–2150.
[28] L. Liu, T. Ning, Y. Ren, Z. Sun, F. Wang, W. Zhou, S. Xie, L. Song, S. Luo, D. Liu, J. Shen, W. Ma, Y. Zhou, Synthesis, characterization, photoluminescence and ferroelectric properties of $PbTiO_3$ nanotube arrays, Mater. Sci. Eng. B 149 (2008) 41–46.
[29] W.F. Zhang, J. Tang, J. Ye, Photoluminescence and photocatalytic properties of $SrSnO_3$ perovskite, Chem. Phys. Lett. 418 (2006) 174–178.
[30] V.M. Longo, A.T. de Figueiredo, S. de Lazaro, M.F. Gurgel, M.G.S. Costa, C.O. Paiva-Santos, V.S. Mastelaro, E. Longo, J.A. Varela, R.W.A. Franco, F.S. De Vicente, A.C. Hernandes, Structural conditions that leads to photoluminescence emission in SrTiO3: an experimental and theoretical approach, Appl. Phys. Lett. 104 (2008) 023515.
[31] B. Henderson, G.F. Imbusch (Eds.), Optical Spectroscopy of Inorganic Solids, Clarendon Press, Oxford, 1989.